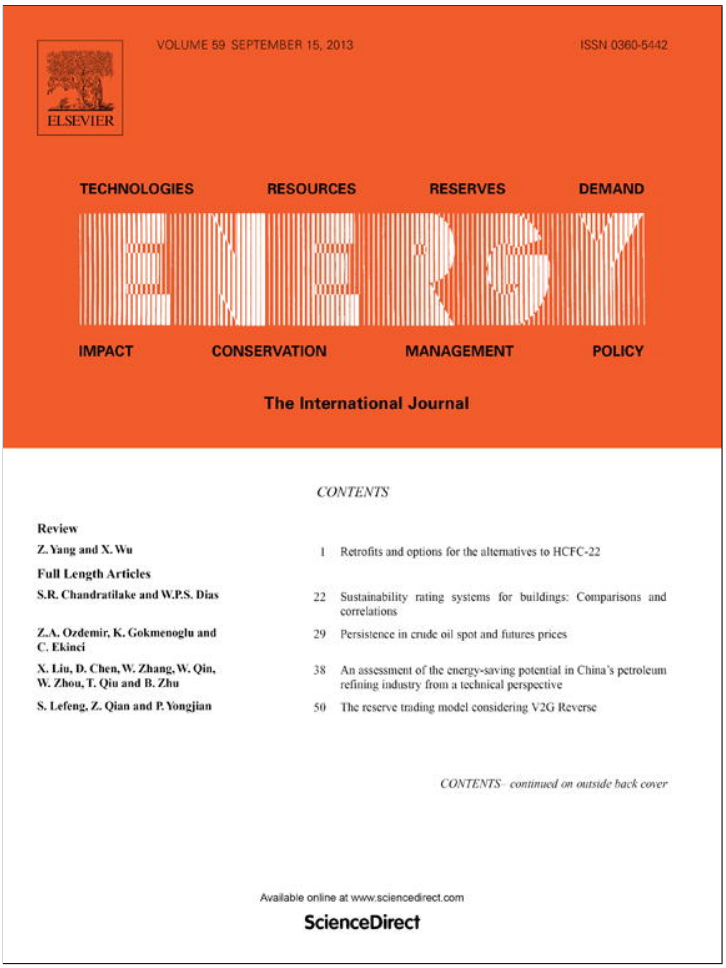

VOLUME 59 SEPTEMBER 15, 2013 ISSN 0360-5442

ELSEVIER

TECHNOLOGIES RESOURCES RESERVES DEMAND

ENERGY

IMPACT CONSERVATION MANAGEMENT POLICY

The International Journal

CONTENTS

Review

Z. Yang and X. Wu 1 Retrofits and options for the alternatives to HCFC-22

Full Length Articles

S.R. Chandratilake and W.P.S. Dias 22 Sustainability rating systems for buildings: Comparisons and correlations

Z.A. Ozdemir, K. Gokmenoglu and C. Ekinci 29 Persistence in crude oil spot and futures prices

X. Liu, D. Chen, W. Zhang, W. Qin, W. Zhou, T. Qiu and B. Zhu 38 An assessment of the energy-saving potential in China's petroleum refining industry from a technical perspective

S. Lefeng, Z. Qian and P. Yongjian 50 The reserve trading model considering V2G Reverse

CONTENTS continued on outside back cover

Available online at www.sciencedirect.com

ScienceDirect

Energy 59 (2013) 83–94

Contents lists available at ScienceDirect

Energy

journal homepage: www.elsevier.com/locate/energy

Shaping array design of marine current energy converters through scaled experimental analysis

A.S. Bahaj, L.E. Myers*

Sustainable Energy Research Group, Energy and Climate Change Division, Faculty of Engineering and the Environment, University of Southampton, Southampton SO171BJ, UK

ARTICLE INFO

Article history:
Received 7 September 2012
Received in revised form
12 June 2013
Accepted 13 July 2013
Available online 21 August 2013

Keywords:
Marine current energy converters
Wake
Array
Turbine

ABSTRACT

Marine current energy converters or tidal turbines represent an emerging renewable energy technology that can provide a predictable supply of electricity. Single devices are in operation around the world with aspirations to deploy farms or arrays of multiple devices.

We present an experimental study that has characterised the downstream wake flow around a 1/15th-scale turbine in a large circulating water channel and a series of experiments involving static actuator disks at 1/120th-scale allowing simulation of multiple-device layouts.

Our analysis demonstrates that the near wake is highly turbulent with structures generated by the rotor and support structure. This region of flow may prove difficult to numerically simulate with a high degree of accuracy. In the far wake the performance of static actuator disks can be matched to mechanical rotors reducing scale and cost facilitating replication of complex array geometries. Here the ambient turbulence and geometric properties of the device/channel drive the wake recovery towards free stream conditions.

Devices operating downstream of others will be subject to a non-steady flow field making comparative performance difficult. We discuss the possibility of unequal device specification and rated power within an array (unlike wind farms) providing a more representative measure of array performance.

1. Introduction

Whilst the concept of extraction of the kinetic energy available in marine currents is a relatively old idea achieving this on a commercial scale has only become a reality in more recent years. Technical advances in related industries such as offshore hydrocarbon extraction and offshore wind energy have increased the knowledge and competency associated with operating in the sea, including underwater actions such as drilling, cable laying and performance of subsea structures. In addition, global desire to reduce the carbon intensity of electricity production provides a clear opportunity to look at natural resources such as marine energy to part of our energy production mix. Previously the drivers for renewable energy arose from the oil crisis of the early 1970's for wind energy and in the 1980's for wave energy where several demonstrator projects were developed. Tidal energy, specifically extracting kinetic energy from flowing waters in the sea (marine currents), represents a recent addition in activities in marine energy conversion. In such conversion, most devices have similar appearance to wind turbines and act in much the same way. However, operation of such underwater turbines is subjected to the strong tidal flows that exist in estuaries, constrained between landmasses and around headlands which are the prime sites for energy conversion. Extraction of kinetic energy from such sites does not require impounding of the operating fluid and as such will have minimum environmental impact as it will maintain almost all of the dynamic nature of the flow. In addition, tidal or marine current energy conversion offers a resource that is predictable in terms of direction and speed translating into a more reliable and quantifiable form of electricity generation compared to more other intermittent renewable energy technologies. Significant resources lay in waters around the United Kingdom [1], North East and North West coasts of the United States and Canada [2], the Philippines and South Korea [3].

1.1. Operations in arrays

Over the last 10 years technology progress of MCEC (Marine Current Energy Converter) technology has undergone various

* Corresponding author.
E-mail addresses: A.S.Bahaj@soton.ac.uk (A.S. Bahaj), luke@soton.ac.uk (L.E. Myers).

0360-5442/$ – see front matter © 2013 Elsevier Ltd. All rights reserved.
http://dx.doi.org/10.1016/j.energy.2013.07.023

development stages from small-scale tank testing through to offshore devices prototype deployment in open seas. Marine energy test centres have been created such as the European Marine Energy Centre in the North of the UK that offer offshore grid-connected berths for tidal turbines in order to test devices, to develop the necessary in-situ knowledge and expertise to quantify performance and energy yields of devices. Recently, successful applications have been made for seabed leases around the UK and elsewhere in the world for MCEC arrays. The projects planned in the UK alone represent an expected installed capacity of over 600 MW by 2020 [4].

The evolution of MCEC arrays is addressed by the authors within the EquiMar protocols on marine energy [5]. Part IIC of these protocols discusses the layout of MCEC arrays with increasing scale of deployment. The most efficient layout in terms of maximising energy extraction and minimising negative device interaction is a single row of devices aligned orthogonal to the mean flow direction (Fig. 1(a)). Unlike wind energy many sites with strong tidal flows are relatively compact in nature often with constrained bathymetry meaning that optimised device layout and packing density is required to extract the maximum amount of energy from a specific site. Hence, a second row can be deployed in an offset manner (Fig. 1b) that will avoid operation in the slower, more turbulent wake flow generated by another device within the array. Depending upon the lateral constraints at any tidal site eventually the increasing number of MCECs will require some devices to operate longitudinally downstream of another (Fig. 1c). Here the inflow conditions are likely to be different to those intercepted by the upstream devices.

Unlike wind energy conversion, the tidal energy resource often has low directionality with flow often reversing by (or very close to) 180° in direction between the flood to ebb tides. Therefore highly geometric array layouts may proliferate if bathymetry is constant across a site. Thus whilst the resource available to each device within the array may vary, the temporal nature will be quite predictable. However, the issue still arises that energy (power) production (whilst predictable) will vary depending upon device position within the array. This predictability might warrant (a) varying device designs, (b) an appropriate control strategy of the array and (c) the quantification of inflow conditions to each device (especially important to those at the centre of the array).

MCEC devices operate by extracting the kinetic energy from the tidal flow and therefore the velocity downstream of the devices will be reduced. This region of slower-moving fluid is termed the 'wake'. Immediately downstream of the device the wake will be at its strongest; a slow, highly turbulent volume of fluid. Fluid mixing will occur between the outer surface of the wake and the free stream fluid that passed around the MCEC. High shear forces at this boundary caused by the disparity in velocity between the wake and ambient flow is one mechanism the second being the turbulent mixing of flow structures present in both the ambient flow passing around the MCEC and structures generated by the device itself (from the rotor blades and device support structure). As we move further downstream the wake becomes wider and the velocity increases such that at a point far downstream the wake has almost completely dissipated and the flow field closely resembles that which existed upstream of the MCEC. A key question is at what longitudinal separation distance should we employ in order to maximise energy capture, minimise operation in turbulent wake flow and hence minimise the cost of electricity generation?

Many different mechanisms and drivers define the structure of the wake as it forms and propagates downstream. The initial strength of the wake principally depends upon the amount of energy extraction but other factors also contribute. As the wake expands downstream the turbulence present in the ambient flow is the key driver for wake dissipation. Other drivers acting to characterise the strength and shape of the wake include the length scales of the system (depth, location and shape of MCEC energy extraction) any bathymetry or seabed roughness features that might affect the global flow field and the form/shape of the MCEC device itself. As such it is a complex flow field; initially it might appear very similar to that downstream of a wind turbine but very different turbulent features and the highly constrained nature of the overall flow field (especially in the vertical plane) have led to highly varied and different wake structures [6].

1.2. Scope of this work

In order to understand the issues mentioned above and pertinent to the MCEC array operation, experimental studies have been conducted to investigate aspects of the flow field that are likely to occur in large arrays. A model (1/15th-scale) horizontal axis MCEC was designed and constructed at the University of Southampton and tested in a large open re-circulating water channel facility. The purpose of this work was the investigation of the near-wake properties of devices and to quantify the longitudinal decay of the wake. This work was augmented by conducting further experiments at 1/120th-scale using static porous membranes or actuator disks. Here the focus was on the characteristics of the far wake region and the performance and flow effects of positioning devices directly downstream of one another as is likely to occur in large MCEC arrays.

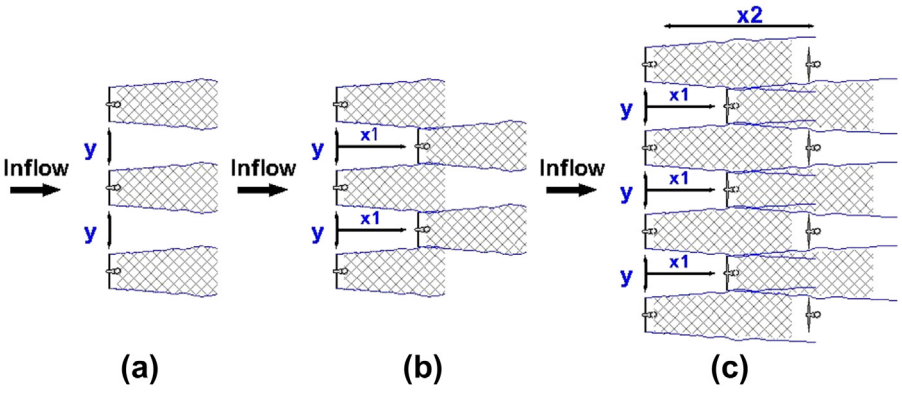

Fig. 1. Plan view of MCEC arrays. (a) Single row, (b) offset dual row, (c) multi-row.

2. Theoretical considerations

2.1. Description of the flow field around a MCEC

The wake of a horizontal axis turbine is commonly separated into two distinct regions; the near and far wake (Fig. 2). The near wake lies immediately downstream of the rotor and is characterised by slow moving fluid (having just passed through the rotor) with strong pressure/shear gradients and intense turbulence structure. Shear stresses are greatest in the annular region close to the blade tips (See Fig. 7). This is principally caused by the motion of the rotating blades and the near wake region is often characterised by a large amount of 'swirl' which for wind turbines has been found to dissipate within 4–5 rotor diameters downstream of the rotor [7,8]. Further turbulent flow features are generated by the static supporting structure. As MCEC technology has not yet stabilized (unlike wind turbines) any structure-generated turbulence is likely to be device-specific.

The transition from the near wake region to the far wake is an important aspect of the flow field. Fluid passing through the rotor will be slowed relative to the ambient flow passing around the rotor. A sheared region of flow will exist at this boundary. As the wake flow begins to expand (in order to conserve momentum) and mixes with the ambient flow the shear layer will move towards the wake centreline (Fig. 2). The downstream distance at which this occurs defines the transition from the near wake to the far wake region.

In the far wake region the device-generated turbulence and rotor swirl is likely to have completely dissipated. The wake continues to expand leading to an increase in surface area that causes the edge of the wake to move outside of the immediate shadow of the device. These two factors lead to increased wake fluid mixing with the faster moving ambient flow that has passed around the turbine rotor. Shear forces serve to mix the outer surface of the wake with the ambient flow, increasing the velocity and narrowing the region of slowest moving fluid about the rotor centreline. Thus the initial momentum deficit caused by the extraction of energy from the fluid by the rotor no longer defines the wake structure or the manner in which it expands downstream but it is the ambient turbulence intensity that is the principal driver for wake recovery.

2.2. MCEC performance parameters and flow properties

Scaling properties of an open channel can present problems at small scale due to the relationship between both the Froude and Reynolds number as given in equations (1) and (2):

$$\mathrm{Fr} = \frac{U}{\sqrt{gd}} \tag{1}$$

$$\mathrm{Re} = \frac{UL}{\nu} \tag{2}$$

Where U is the flow velocity, g is the acceleration due to gravity, d is the water depth, L is the characteristic length (generally taken as the depth for wide channels) and ν is the kinematic viscosity of the fluid. The Froude number represents the ratio of inertia to gravitational forces and is pertinent when there is a free surface in close proximity to the model in question. Here the length term is always the channel water depth. Channel Froude number should be maintained at large and small scale to ensure the channel dynamics are comparable in terms of water surface elevation. The Reynolds number is the ratio of inertia to viscous forces and governs the performance of the blades in terms of lift/drag ratio and hence power and thrust acting upon a rotor.

If we assume the same fluid is used in at large/small scale and that the acceleration due to gravity is constant then we can define a velocity ratio for the Froude number:

$$V_\mathrm{r} = \sqrt{d_\mathrm{r}} \tag{1a}$$

And similarly for the Reynolds number:

$$V_\mathrm{r} = L_\mathrm{r}^{-1} \tag{2a}$$

Thus linear scaling of both these parameters cannot be achieved when the model/prototype ratio becomes too small.

Discrepancy in Reynolds numbers between model and prototype is usually tolerated for the scaling of hydraulic channels if Froude similarity is maintained and both full-scale and model Reynolds numbers lie within the same turbulent classification. It has been demonstrated previously [9] that for mechanical tidal turbine rotors the blade rotor performance (power and thrust) is

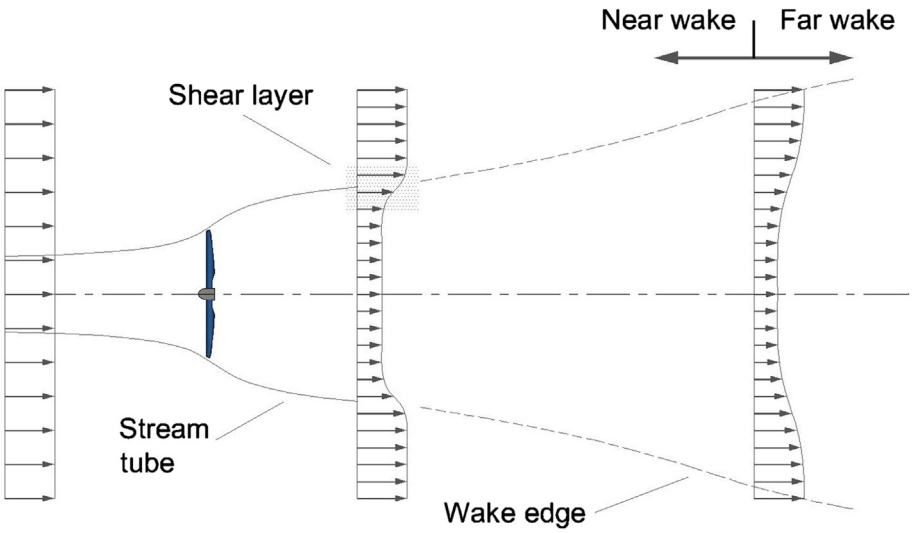

Fig. 2. Illustration of the transition from the near to far wake.

independent of Reynolds number when in excess of 5×10^5 i.e. the flow can be classified as turbulent.

In a similar manner the influence of a submerged obstruction on the water surface elevation is independent of Froude number when less than 0.25. Nearly all relatively deep tidal channels have Froude numbers less than 0.25. Above this undular waves and surface instabilities might occur around a model MCEC that are unlikely to occur at full-scale. Therefore parity in Froude number was employed in this work whilst Reynolds numbers across the MCEC rotor blades were fully turbulent.

In order to normalise the fluid velocity in the wake to the ambient inflow a velocity deficit is defined. This is a non-dimensional number relative to the longitudinal free-stream flow speed (U_0) at a position 3-diameters upstream of the MCEC and with the same lateral and vertical position as a corresponding point in the MCEC wake where the longitudinal velocity is defined as (U_w):

$$U_{\text{deficit}} = 1 - U_w/U_0 \tag{3}$$

Turbulence intensity, I is defined as the root-mean-square of the turbulent velocity fluctuations with respect to the mean velocity and is calculated by:

$$I = \frac{\sqrt{\frac{1}{3}\left(\overline{u'^2} + \overline{v'^2} + \overline{w'^2}\right)}}{\sqrt{U^2 + V^2 + W^2}} \tag{4}$$

Where U, V, W denotes mean velocity components in the longitudinal (x), lateral (y) and vertical (z) directions. u', v', i' represent the varying component of velocity (mean minus instantaneous). As the longitudinal velocity component (x) dominates the mean velocity (lateral (y) and vertical (z) velocities are very small) the separate component turbulence intensities are often given to give a more complete picture of the flow conditions.

Horizontal and vertical shear stresses are defined as:

$$\text{HSS} = -\rho\overline{u'v'} \tag{5}$$

$$\text{VSS} = -\rho\overline{u'w'} \tag{6}$$

Where ρ is the fluid density.

Axial momentum theory has long been used to characterise and define the operation and some performance parameters of horizontal axis turbines that extract kinetic energy from a fluid across a plane orthogonal to the principal flow direction. The near wake velocity deficit is strongly influenced by the momentum drop across the rotor disk which the theory defines as:

$$U_w = (1 - 2a)U_0 \tag{7}$$

The parameter a is the axial induction factor, a measure of the decrease in fluid velocity though the rotor plane. This has been shown to have a maximum value of 1/3 for an un-augmented rotor operating in an incompressible flow [10]. From axial momentum theory a dimensionless coefficient of thrust can be defined:

$$C_T = \frac{\text{Thrust}}{0.5\rho U_0^2 A_d} = 4a(1 - a) \tag{8}$$

Where A_d is the area of the rotor and a is the axial induction factor. It applies equally to horizontal axis wind turbines and MCECs, the only difference being the fluid density and typical operating flow speeds. Thrust values for marine turbines per unit area are approximately 50 times greater than wind turbines (at typical operating flow speeds) and 5 times greater for typical rotor swept areas. For increasing rotor thrust the initial wake velocity deficit should increase until $a = 0.3$ and $C_T = 0.9$. C_T values in excess of 0.9 are possible at which point actuator disk theory breaks down and empirical relationships can be substituted [11].

Similarly a coefficient of power can be defined:

$$C_P = \frac{\text{power}}{0.5\rho U_0^3 A_d} = 4a(1 - a)^2 \tag{9}$$

Again taking a maximum value of $a = 1/3$ the theoretical maximum power coefficient will be equal to 16/27 or 0.593 as predicted by Betz and often referred to as the Betz limit.

3. Experimental set up

The experimental programme covers two separate but connected phases which are designed to impart some of the needed understanding of the salient issues of array design and operation albeit at model scales. The work covers energy extracting model turbines and static actuator disks. A summary of the experimental set up and processes is given in the following sections.

3.1. Turbine design

Previous experimental studies [9,12,13] have demonstrated that there is an acceptable minimum scale for horizontal axis turbines in order to maintain appropriate levels of thrust, power and to ensure representative water surface profiles. In order to fulfil such conditions, a representative turbine scale, having a rotor diameter of around 800 mm was chosen to maintain the ratio of MCEC diameter to water depth so far seen for many full-scale prototype MCEC devices installed around the world. This scale also ensured that Reynolds number along the blades was sufficiently high enough to avoid large regions of laminar flow. Hub diameter of the rotor was 100 mm with the main nacelle body measuring 114 mm in diameter. The blades were composed of NACA 48XX aerofoil sections for good lift/drag performance at lower Reynolds numbers and delayed stall characteristics. Blade design details are given in Table 1A in Appendix A. Peak rotor C_P was measured at 0.45 at a rotor tip speed ratio of 6, values close to those of full-scale devices. The turbine consisted of a three bladed rotor attached to a main shaft driving an axial transmission fully contained within a tubular nacelle (Fig. 3a). A streamlined tapered section with an aspect ratio of approximately 3 was placed on the vertical support tower in order to reduce the turbulence from the cylindrical tower section into the near wake region generated by the rotor. A gearbox was used to increase the rotational speed (reducing torque) for the generator which was located at the rear of the nacelle.

An in-line strain gauge dynamometer mounted immediately behind the rotor hub, and running wet, was used to measure the rotor thrust. There was sufficient torsion in the aluminium shaft to measure rotor torque by directly gauging the inner surface of the hollow shaft. The dynamometer (Fig. 3b) was CNC machined from solid Aluminium bronze. The rotor hub was in contact with the outer rim of the dynamometer meaning that thrust force was transmitted to the drive shaft via 4 members bending in contra-flexure. Strain gauges were laminated to these flexures in a full bridge circuit arrangement.

A wireless data telemetry system was employed to convey signals from the turbine. The system included means to smooth, amplify and digitize outputs directly from the bridges to ensure maximum data quality and accuracy. The power take-off subsystem consisted of a planetary gearbox and permanent magnet generator and an optical sensor to measure the rotational speed. Electrical

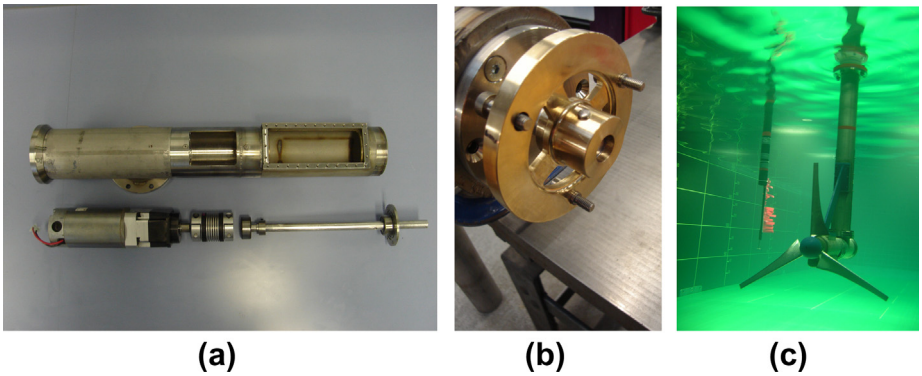

Fig. 3. Model scale MCEC. (a) Nacelle and power take-off subsystem, (b) detail of thrust dynamometer, (c) MCEC model device operating in a circulating water channel facility.

power generated by the turbine was dissipated above the waterline via an umbilical cord that also conveyed rotor data and power for the telemetry system. An image of the turbine installed in the water channel is shown in Fig. 3c.

3.2. Actuator disks

Smaller scale testing was required for studies involving device interaction and the study of the wake effects far downstream from the simulators. In this phase of the works, static porous actuator disks of 100 mm diameter were mounted in the flow using a rig that incorporated a variable pivot arrangement to mechanically amplify the small thrust forces acting upon the disks. A range of disk porosities were used to replicate the varying thrust coefficient acting upon a rotor over a range of tip speed ratios. The use of actuator disks has been demonstrated before for wind turbine applications [7,14] and also for marine applications [15,16] in which the similarity between rotors and static disks were discussed at length. In addition, justification of non-rotating disks has been made for study of the far wake region where the ambient flow field is the principal driver of wake recovery, not the thrust force or turbulence generated by the MCEC device. Comprehensive description and discussion of the actuator disk scaling and arrangement presented herein can be found in Ref. [15].

3.3. Experimental facilities and device set up

The 1/15th-scale model MCEC was tested in the IFREMER circulating water channel, Boulogne-sur Mer, France. The turbine was mounted 4 m from the inlet of the channel working section. Total channel length was 18 m with approximately 8 m available for flow measurements due to constraints within the facility. Fig. 4 gives the remaining key dimensions of the position of the rotor within the channel.

The turbine was mounted close to mid-depth during all experiments. The vertical blockage ratio (channel depth/rotor diameter) was set to replicate that expected for full-scale devices, between 2.5 and 3 depending upon total channel depth. The blockage ratio of the MCEC device in the channel was 6.3%.

In order to minimise any deformation of the water surface the channel was run at a Froude number close to that of a real tidal channel. This was balanced with the need to select an operating velocity high enough to allow a full range of blade tip speed ratios to be achieved. Based upon these drivers a depth-averaged flow speed of 0.78 m/s was chosen with a corresponding Froude number of 0.176. Ambient turbulence in the flume was approximately 6–8% along the longitudinal and lateral axes. Vertical intensity was lower at approximately 2%. This was attributed to the shape of the inflow section and the inclusion of flow-straightening elements.

The actuator disk experiments were conducted in a smaller flume at the Chilworth hydraulics laboratory, University of Southampton, United Kingdom. The channel is a conventional gravity fed flume with a working section 21 m in length, 1.35 m width and depths up to 0.5 m. For this work channel Froude number was maintained at 0.175. Turbulence intensity was in the range of 6–8% longitudinal and lateral components whilst the vertical intensity was 3–4%. The vertical velocity profile is fully-turbulent in nature [14].

In both experimental cases the ratios of turbulence intensities were similar to those observed in a full-scale tidal channel [17] where the ratio of intensity (x:y:z) was quantified in the Sound of Islay UK at 1:0.96:0.67. However it is acknowledged that this ratio

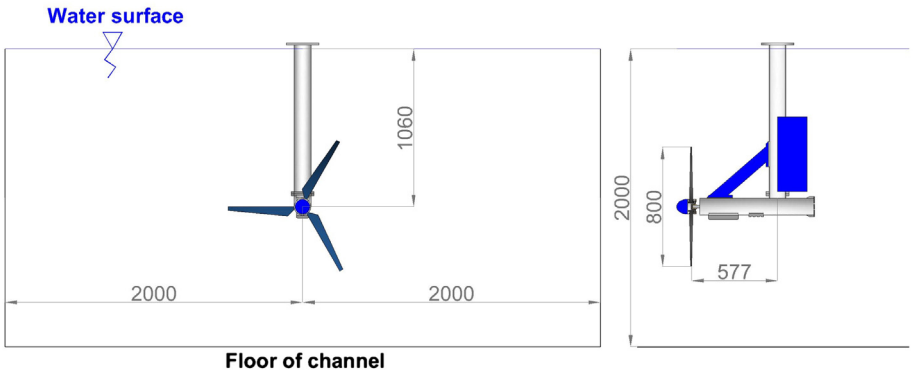

Fig. 4. Front and side elevation of the position and dimensions of the 1/15th-scale MCEC in the circulating water channel (all dimensions in mm).

and the magnitude of turbulence will no doubt be highly site-specific.

3.4. Flow characterisation

Both ADV (Acoustic Doppler Velocimeters) and LDV (Laser Doppler Velocimeters) were used to characterise the flow fields around the mechanical turbine and static actuator disks. The lower cost and greater operational flexibility of ADVs has seen a proliferation in use during recent years. Comparative performance between ADV and LDV systems has been assessed previously [18,19]. Mean flow velocity and estimates of Reynolds stresses were found to agree to within 1%. Laser systems whilst offering enhanced temporal and spatial resolution are more expensive and often only acquire data along 2 axes. The LDV used in this work also required a long period of time to acquire data based upon the on-board processing employed to ensure good data quality.

All data sets were post processed in order to remove any spurious data points. Low return signal strengths of very turbulent flows can lead to spiking and recording of events that are unlikely to be actual measured flow features. For this work a velocity cross-correlation filter was applied [20].

Removed points were not replaced thus the filtered sample set was simply truncated. Sampling for an extended period with the ADV ensured that the remaining data sets were of a sufficient size that higher order flow parameters such as turbulence intensity, energy spectra etc. could be accurately resolved. Through particle seeding and filtering data sets both instruments agreed within appropriate limits (accounting for small difference in sample standard deviation, repeatability, probe location and shear across the larger ADV sample volume). Fig. 5 shows a lateral (cross-channel) line of measurements taken in the large circulating channel at 1060 mm depth (rotor hub height) under ambient operational flow conditions in the absence of the turbine. The effect of removing spikes from the datasets and increased particle seeding offer a clear improvement in measurement agreement between the ADV and LDV.

Correct interpretation and processing of data is most important in more turbulent flows where return signal strengths are reduced further. Again, the accuracy of higher order flow effects suffer more as the nature of velocity spiking tends to be a number of errors that are equally positive and negative. Thus the mean velocity of a sample not greatly affected but the increase in sample energy will affect values of shear stresses, turbulence intensity and turbulent kinetic energy to a much greater extent. Fig. 6 shows raw and filtered vertical shear stress at 5-diameters downstream of the model MCEC rotor centreline. Vertical position is expressed in normalised rotor diameters (D) from the centreline or hub position. The effect of the filtering is to reduce the high-energy events and also to smooth the data; this is achieved not through a filter per-se but rather by rationalising true data points and removing those not falling within the criteria specified such as having too great an instantaneous acceleration etc. The filtered data (right) shows high differential shear stresses corresponding to the rotor blade tips, in this case 5-diameters downstream at a vertical location approximately $\pm$0.5 diameters. Each line represents a different lateral location so here an approximation of the lateral extent of the wake can be made. At 0.8 and 1.0D lateral offset the profiles are relatively linear which correspond to the ambient channel conditions.

Using several hundred point velocity measurements the mean velocity across the rotor plane was calculated to be 0.788 m/s. This value was used for the determination of rotor thrust and power coefficients. A similar plane of measured data was acquired for the actuator disk experiments. Comprehensive wake measurements were then made downstream of the turbine and actuator disks.

4. Results and discussion

4.1. Near wake properties of a horizontal axis MCEC

Whilst the far wake region is undoubtedly of great importance to inter-device spacing within an array there is still a requirement to understand the flow development within the near wake region. Lagrangian and Eulerian computational fluid dynamic numerical models often solve in a downstream direction commencing in the vicinity of the rotor. The combination of turbulent flow structures shed from the MCEC support structure and the rotating blades will complicate the near wake flow field and could lead to reduced accuracy when modelling the important far wake region. To establish a clear indication of this, the wake shed by a model horizontal axis turbine has been measured with (a) the rotor inoperative to assess the nature of the flow field and (b) the rotor in operation to characterise the near wake region and to investigate the effects further downstream into the far wake.

Fig. 7 shows the vertical centre plane velocity from 2.5 to 5 diameters downstream (rotor inoperative) that has a number of interesting features. The lower of the two triangular flow structures, centred at a vertical offset of 0D, is shed from the rear of the cylindrical nacelle. The upper structure is at the same depth as the cross reinforcement strut mounting on the upstream face of the

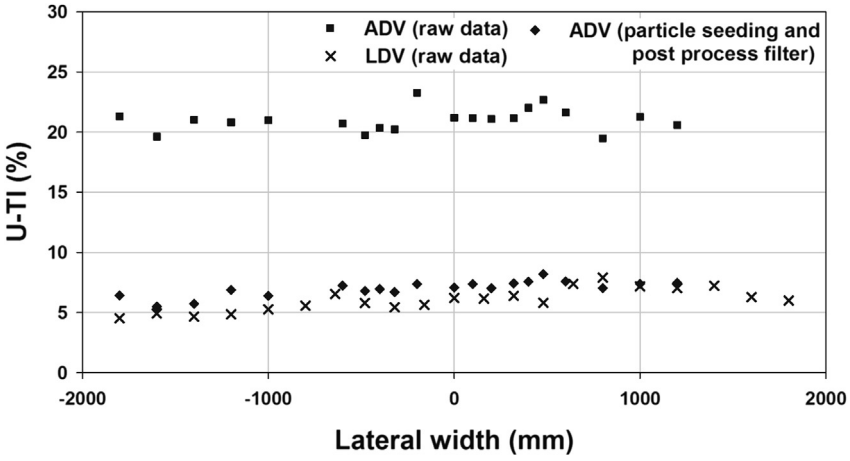

Fig. 5. Agreement of turbulence intensity between ADV and LDV instruments following particle seeding and data post processing.

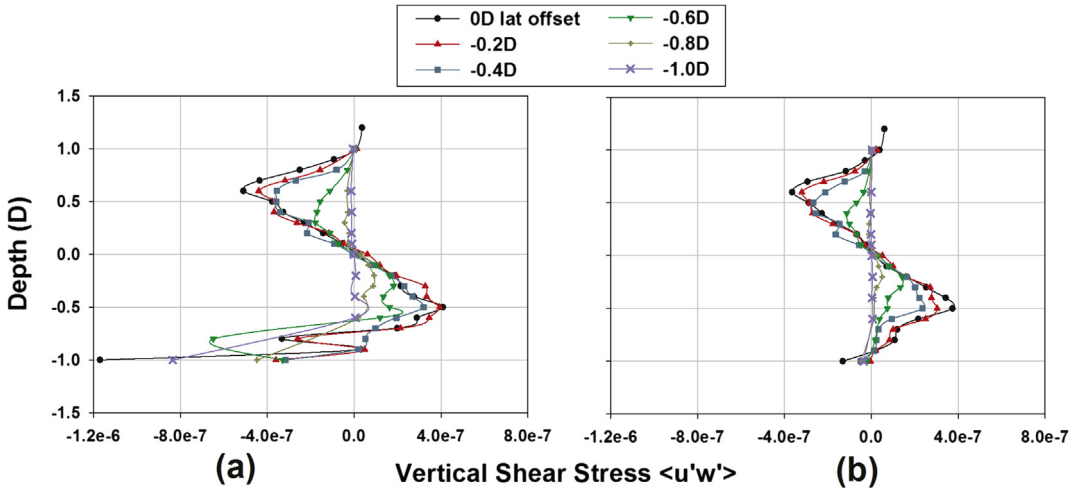

Fig. 6. Vertical shear stress 5-diameters downstream of 0.8 m MCEC, (a) raw data and (b) filtered data.

vertical tower section. Despite the presence of the short streamlined section on the vertical tower a wake is still formed that persists to almost 4*D* downstream of the rotor. Closer to the water surface the circular tower section creates a wake that persists further downstream. It can be concluded that the near wake may be strongly influenced not only by the wake formed by the MCEC power capture subsystem (rotor) but also by the supporting structure. Until the technology becomes stabilised, such is the case for wind turbines (3-bladed horizontal axis turbines), this additional velocity deficit and added turbulence will be specific to each type of device which makes generic modelling of the near wake region difficult.

As discussed previously the near wake is strongly influenced by the initial momentum drop across the rotor plane. This is expressed through the dimensionless rotor thrust coefficient. With the rotor now operational Fig. 8 shows the centreline vertical velocity deficit profiles measured at 5-diameters downstream for 3 different values of rotor thrust coefficient. Close to the rotor hub depth the inverse relationship between velocity and rotor thrust coefficient can be seen to good effect even at this downstream location close to the transition between near and far wake. It also shows that the rotor thrust has a bearing on the velocity deficit across a region within the rotor diameter ($\pm 0.5D$). The upper and lowermost parts of the wake are more asymmetrical in keeping with the presence of the MCEC support structure occupying a region from $-0.1D$ up to the water surface. The effects of the wake shed from the vertical cylindrical tower are still evident nearer to the water surface at 5-diameters downstream. The velocity beneath the rotor has increased relative to the ambient inflow velocity where the deficit can be seen to be less than zero. This is attributed to the low vertical blockage as the rotor occupies 40% of the total depth and thus fluid is constrained between rotor and bed leading to an increase in velocity relative to the inflow.

The turbulence generated from the combined rotor and MCEC support structure is shown in Fig. 9. The vertical tower piercing the water surface combines with the rotor wake removes radial symmetry about the rotor hub. Near wake characteristics quantified herein have implications for numerical models trying to characterise the near wake or commencing at the rearward edge of the near wake. It is clear that validation data from real devices will include elements of flow influenced by the turbine support structure.

Fig. 10 shows the lateral velocity measured downstream of the turbine at centre-depth when operating at a rotor thrust coefficient of 0.77. By inspection it can be said that the shear layer reaches the wake centreline between 5 and 6 diameters downstream, approximately in agreement with values quoted for wind turbines [21].

The transition point is of importance for numerical models which must take into consideration the different driving mechanisms for wake formation, expansion and recovery. We have seen from Fig. 8. That the rotor thrust and device support structure has a strong bearing on near wake properties. In this study the agreement with the transition point found for wind turbines is likely due to the relatively low turbulence intensity in the water channel. Real sea conditions could well be far more turbulent with varying length scales and rates of generation in which case the transition point may be closer to the MCEC as the ambient turbulent features penetrate into the near wake and lead to the shear layer reaching the rotor centreline much earlier.

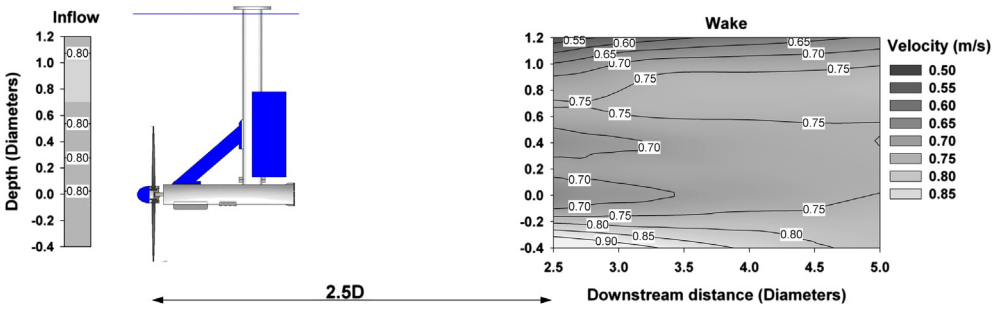

Fig. 7. Vertical centre plane velocity field downstream of MCEC with rotor static.

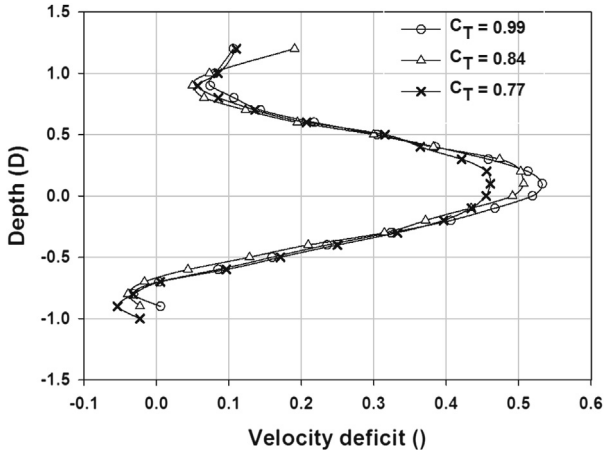

Fig. 8. Centreline vertical velocity profiles 5-diameters downstream of operational MCEC device at varying levels of rotor thrust coefficient.

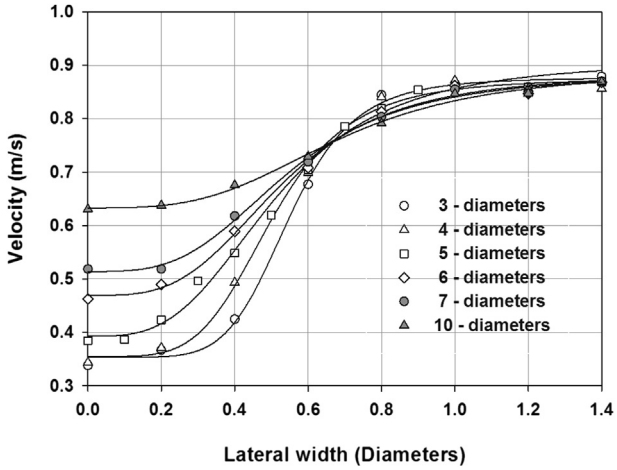

Fig. 10. Lateral velocity measurements downstream of MCEC at rotor centre height.

4.2. Far wake properties and longitudinal spacing of MCECs

Actuator disks of 100 mm diameter were mounted with a geometrically scaled support structure replicating that of the turbine (Fig. 11). Channel dimensions were geometrically scaled down such that the actuator was operating in 2.5-Diameters depth and 5-diameter channel width and with Froude similitude of the larger scale rotor experiments. Channel turbulence intensities were given in section 3.3.

Fig. 12 shows the centreline and lateral velocity deficits from both the rotating 1/15th-scale MCEC and a 1/120th-scale actuator disk for different operating rotor thrust coefficients. The disparity in the centreline near wake velocity deficits can be attributed to the differing nature of flow entrainment through each type of device. For a mechanical rotor the blades serve to rotate the wake about the hub axis hence there is a degree of swirl which promotes mixing in the near wake up to approximately 3–4 diameters downstream. For the actuator disk the initial reduction in velocity is much greater (for comparable rotor thrust coefficient) which is attributed to the lack of wake rotation and the small-scale turbulence generated from the small apertures. Therefore the initial deficit (at 3*D* downstream) appears greater for the actuator disk despite comparable values of C_T. Indeed flow visualisation directly downstream of the actuator disks shows a region of very stagnant fluid between 1 and 3 diameters downstream. As the far wake region is approached and further downstream, the velocity deficit of the actuator disk and mechanical rotors converge. This can be seen to good effect on the lateral velocity deficit profiles. This indicates that the near identical ambient turbulence of both water channel facilities is the principal mechanism for wake recovery coupled with the identical lateral geometries of devices, and proximity to sidewalls, channel floor and water surface. This result demonstrates that the use of actuator disks is an acceptable approach for modelling of arrays when far wake conditions are required to be understood. However C_T values for the static disks could be slightly lower than for the mechanical rotors to correct for the larger initial reduction in velocity downstream of the static disks. Replication of ambient turbulence, rotor disk thrust coefficient, Froude number similitude and geometric length ratios (lateral/vertical blockage) should all be observed. Advantages for this approach are that the working length of a channel required to study longitudinal arrangements of devices can be reduced from 12 to 20 m (for a 1:15th-scale turbine) to somewhere in the order of 3 m (for 1:120th scale actuator disks).

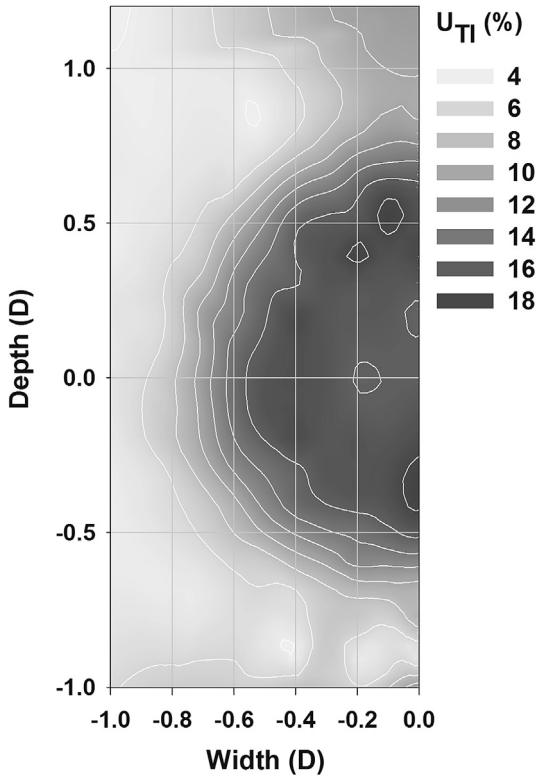

Fig. 9. Longitudinal turbulence intensity measured across a lateral plane 5-diameters downstream of an operating MCEC.

The experimental work was extended to the investigation of the wake formed from a device whilst operating in the wake on another as reasoned by discussion around Fig. 1(C) earlier. A 100 mm actuator disk (upstream) was placed at centre depth in the Chilworth flume in water 3-diameters deep. The wake from the disk was comprehensively measured in all three dimensions. Another single actuator disk was then placed at 7*D* downstream from the upstream disk and the wake generated from the downstream disk was subsequently measured. A key issue here is that the upstream disk is positioned in an isotropic flow field whilst the downstream disk is positioned in a flow field that is constantly changing with longitudinal position due to the decaying wake flow created by the upstream disk. The longitudinal distance of 7-diameters was

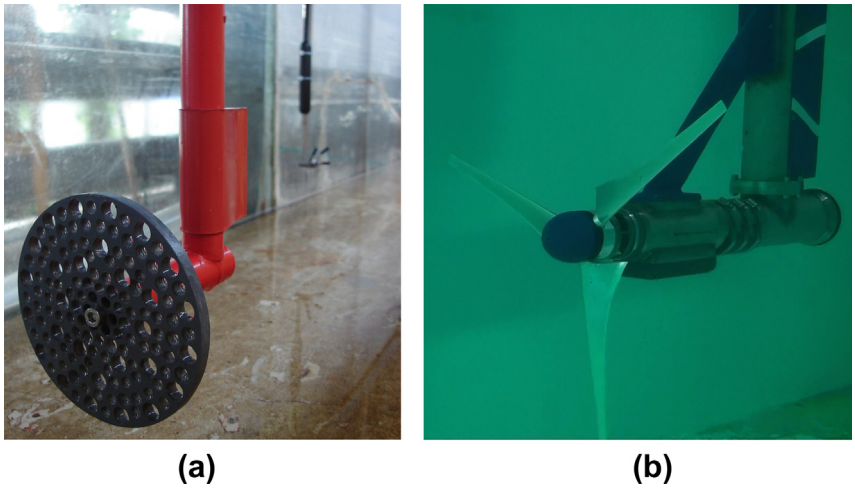

Fig. 11. Actuator turbine (a) and rotating mechanical device (b).

chosen as being within the far wake region whilst also at a downstream distance influenced by the upstream device.

Fig. 13 shows both the normalised velocity deficit and turbulence intensity for the wake generated by the upstream disk and the combined flow field downstream of the second disk. Note that the velocity deficit (upper plots) is normalised with respect to the flow far upstream of the upstream disk. The wake decay from the upstream disk can be clearly seen persisting well into what will become the far wake region of the downstream actuator disk. The majority of the added turbulence intensity created by the upstream disk tends to dissipate by 10–12*D* downstream. This would suggest that the wake of the downstream disk might not dissipate any faster especially in the far wake region.

The centreline velocity through both actuator disks arrangement is shown in ">Fig. 14. All distances are relative to the upstream disk with the value at 0*D* representing the inflow velocity to the upstream disk. The sharp reduction in velocity in the very near wake can be seen with the subsequent initiation of wake velocity recovery occurring as the flow approaches the downstream actuator disk. The inflow velocity at the downstream disk is some 13% lower than for the upstream disk. This translates to a 35% reduction in available inflow energy across the downstream disk compared to that positioned upstream.

Estimation of the axial induction factor from momentum theory will allow a crude quantification of the observed velocity reduction across the disk. This is done with the obvious caveat that calculation of the immediate wake velocity will differ between an actuator disk and horizontal axis rotor (due to the differing characteristics of the near wake as discussed above). Disk C_T was quantified using the inflow velocity to each disk. For the downstream disk this was taken as the velocity at the disk location but in its absence. Values for the upstream and downstream disks we found to be 0.8 and 0.82 respectively which seemed reasonable considering the identical porosity and structure of both. Using equations (7) and (8) to determine U_w (initial near wake velocity) and substituting $a = 0.28$ for the upstream disk and $a = 0.29$ for the downstream disk (based upon the measured disk C_T) the predicted values of U_w for the upstream and downstream disks are 0.136 m/s and 0.102 m/s respectively. The higher than predicted initial near wake velocity for the downstream disk may be attributable to the increased turbulence generated by the upstream disk that propagates into the near wake of the downstream disk. This turbulent flow could serve to dissipate the stagnant fluid that is usually present up to 3*D* downstream of the actuator disks.

The rate of far wake velocity recovery for both disks was expected to be similar and this is shown to good effect in Fig. 14. The initial rate of recovery for the downstream disk is greater but from approximately 20 diameters onwards (13*D* from the downstream disk) the rates of recovery are comparable. This is the region where wake recovery is driven by ambient turbulence and as can be seen from Fig. 13 any added turbulence from the upstream disk has broadly dissipated at this downstream distance.

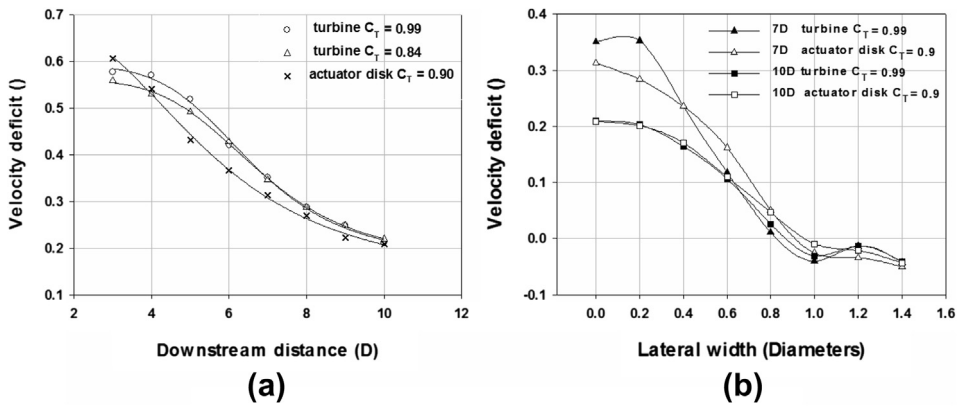

Fig. 12. Comparison of downstream velocity deficit of actuator disk and energy extracting turbine for axial centreline (a) and lateral centre-depth (b).

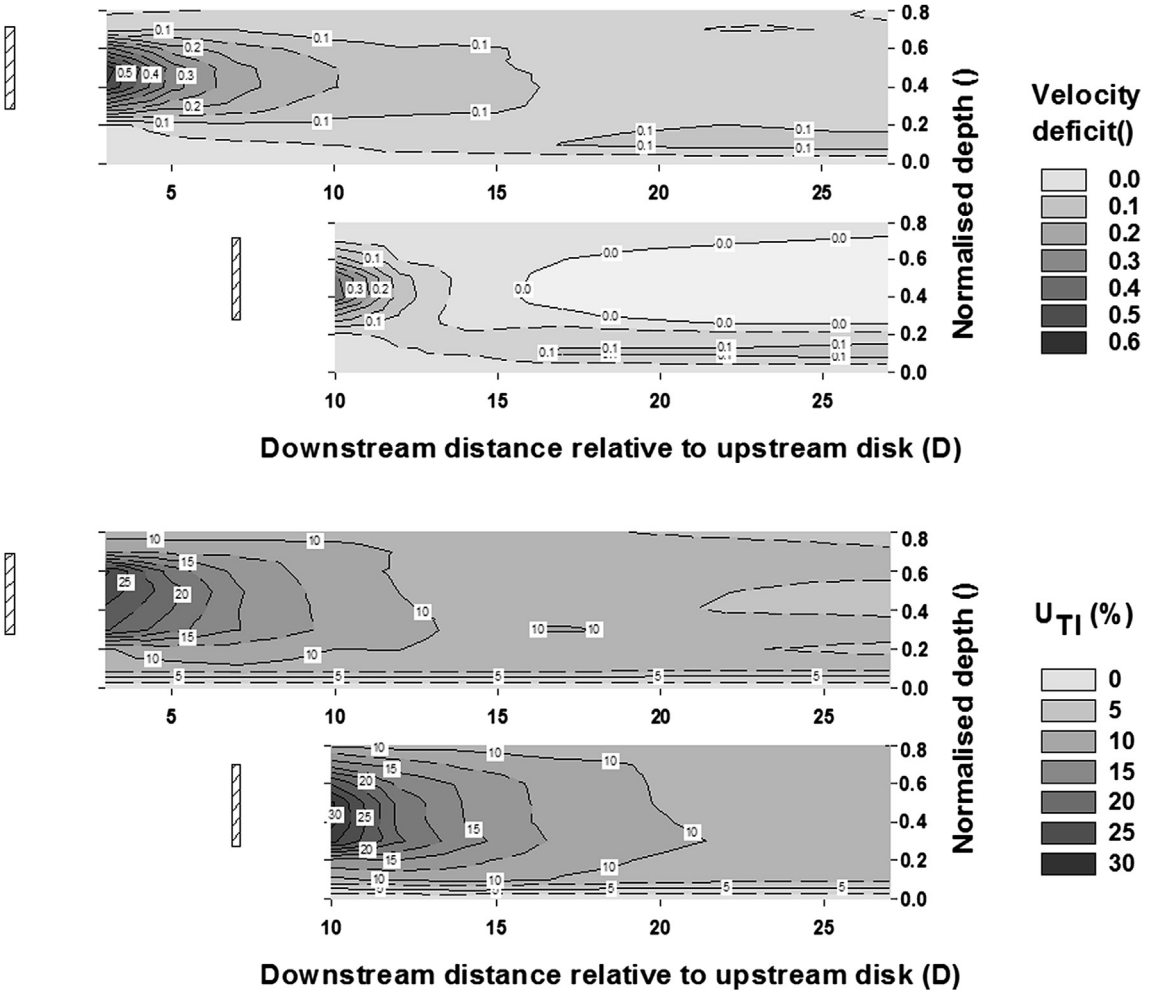

Fig. 13. Downstream vertical centre plane flow field of a two actuator disks aligned longitudinally one upstream and the other at 7-diameter spacing downstream. Normalised velocity deficit (upper plots) and turbulence intensity (lower plots).

For full-scale devices in the sea it remains to be seen whether smaller length scale turbulent flow structures generated by an MCEC dissipate before it can affect the wake of a downstream device. Compared to these smaller scale studies the few offshore measurements in strong tidal flows have measured longer length scale ambient turbulence and generally higher turbulence intensities [22]. This may facilitate more complete wake mixing such that downstream centreline velocity recovery is more rapid

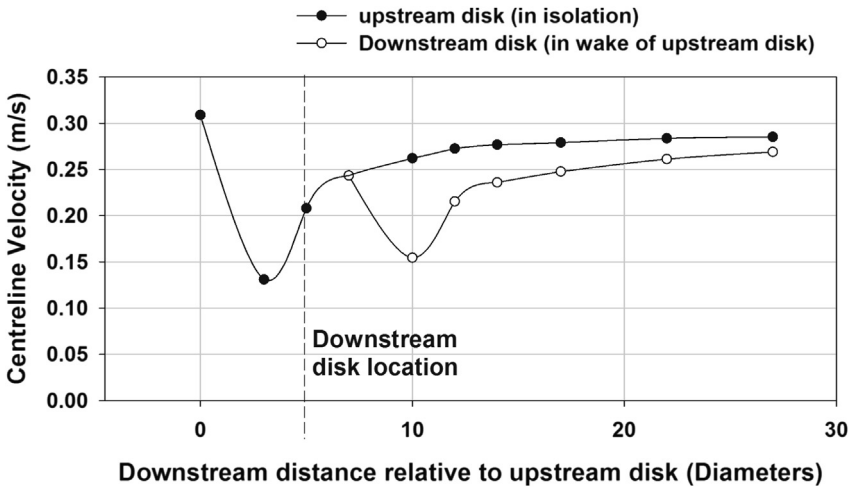

Fig. 14. Centreline velocity profiles of 2 actuator disks aligned longitudinally one upstream and the other at 7-diameter spacing downstream.

allowing closer device spacing. It should be remembered that tidal energy sites are generally unique in terms of tidal forcing and turbulence-generating bathymetric features. Therefore there is unlikely to be a general rule for spacing MCEC devices as opposed to those that seem to exist for offshore wind farms.

4.3. Normalisation of MCEC performance parameter when arranged in arrays

Expressing performance parameters in terms of dimensionless coefficients or ratios is found to be a sound method for assessing comparative performance of both different types of device and similar devices operating under varying conditions [5]. Normalising flow speeds within a multi-row array will present certain difficulties due to the non-uniform nature of the flow field downstream of MCEC devices.

A further issue related to the rated power of devices within an array. Power production from devices deep within the array will likely be lower than those in the first upstream row due to the lower inflow speeds due to energy extraction from upstream devices. If we take an "all devices are equal approach" the array instantaneous power production and the electrical load factor will be artificially low. As the tidal energy resource is predictable in terms of direction and speed it may be possible to manage devices with different performance parameters. Indeed there may be some financial advantage to down-rating power output of devices deep within an array. Higher electrical load factors are also more desirable in terms of management of the onshore electrical grid and in some countries also command greater financial reward for predictable and more steady electricity generation. Clearly this is not as practical for wind farms where the wind direction is far more varied and unpredictable but for almost bi-directional tidal currents and highly geometric layouts of MCECs within an array it could be considered, especially for large arrays.

5. Conclusions

A comprehensive experimental campaign has been conducted to characterise the downstream wake of marine current energy converters through the use of energy extracting model rotors and static actuator disks. Discussion of array evolution points to relatively geometric arrangements of devices depending upon the directionality of the resource and the bathymetric profile at any particular site. For demonstrator arrays with installed capacity around 10 MW it should be relatively easy to avoid any negative interaction between devices. For multi-row arrays this will become increasingly difficult and operation in turbulent wake flow for devices at the centre of the array is likely.

The initial reduction in velocity downstream of an MCEC has been shown to depend upon the rotor thrust coefficient and the near wake region is characterised by strong turbulence features generated by the rotor and device support structure. These effects can combine and persist downstream close to the region at which the transition from the near to far wake condition exists. This has implications for numerical models that might use approximations to define the complex near wake in order to commence simulations in the more easily resolved far wake region.

In the far wake velocity recovery is predominantly driven by the ambient turbulence. A comparison between energy extracting rotors and static actuator disks simulators shows that for identical geometric ratios and very similar ambient turbulence characteristics the rate of velocity recovery in the far wake recovery is comparable. This finding will facilitate more manageable and cheaper experimental studies to be conducted with actuator disks.

Our observation from actuator disk experiment indicates that operation of devices arranged axially downstream of each other reveals that the added turbulence from an upstream device can aid the wake recovery of a device located downstream. However, array spacing is likely to be strongly driven by two opposing factors; firstly to consider the cubic relationship between available kinetic energy and velocity for a downstream device and secondly to maximise the energy acquired per unit area for any MCEC array. Defining wake recovery within an array is most easily expressed in an absolute fashion via velocity data. Approaches to normalising data within an array can lead to non-comparable datasets unless spatially varying flow data is used for normalising purposes. Whilst this is arguably more representative of true performance there are practical implications in obtaining sufficient data in terms of cost and spatial resolution of offshore measurements.

Acknowledgements

This work was part of a project funded by the Department of Business, Enterprise and Regulatory Reform on performance characteristics and optimization of marine current energy converter arrays, BERR Project number T/06/00241/00/00. The work addressing classification of arrays was part of 'Equimar', funded under the European Community's Seventh Framework Programme FP7/2007-2013 under grant agreement number FP721338.

Appendix A. Supplementary data

Supplementary data related to this article can be found at http://dx.doi.org/10.1016/j.energy.2013.07.023.

References

[1] Carbon Trust. Phase II tidal stream resource Report; July 2005.
[2] Bedard R, Presivic M, Polaye B, Casavant A. North America tidal in-stream energy conversion technology feasibility study. Electrical Power Research Institute (EPRI); 2006 report number EPRI_TP-008-NA.
[3] Jo CH, Kang Hee L, Yu Ho R. Recent TCP (tidal current power) projects in Korea. Science China Technological Sciences 2010;53:57–61.
[4] Bahaj AS. Generating electricity from the oceans. Renewable and Sustainable Energy Reviews 2011;15:3399–416. http://dx.doi.org/10.1016/j.rser.2011.04.032.
[5] EquiMar. Equitable testing and evaluation of marine energy extraction devices in terms of performance, cost and environmental impact. Part II C. In: Ingram D, Smith G, Bittencourt-Ferreira C, Smith H, editors. Edinburgh, United Kingdom: University of Edinburgh, School of Engineering; 2011, ISBN 978-0-9508920-2-3; 2011.
[6] Myers LE, Bahaj AS, Germain G, Giles G. Flow boundary interaction effects for marine current energy conversion devices. In: Proceedings of the 10th world renewable energy congress, Glasgow, United Kingdom 2008.
[7] Sforza PM, Sheerin P, Smorto M. Three-dimensional wakes of simulated wind turbines. American Institute of Aeronautics and Astronautics Journal 1981;19:1101–7.
[8] Connel JR, George RL. The wake of the MOD-0A1 wind turbine at two rotor diameters downwind on 3 December 1981; 1981. US DOE Report, no. PNL-4210.
[9] Mason-Jones A, O'Doherty DM, Morris CE, O'Doherty T, Byrne CB, Prickett PW, et al. Non-dimensional scaling of tidal stream turbines. Energy August 2012;44(1):820–9.
[10] Betz A. Das maximum der theoretisch möglichen ausnutzung des windes durch windmotoren. Gesamte Turbinenwesen 1920;17:307–9.
[11] Burton T, Sharpe D, Jenkins N, Bossanyi E. Wind energy handbook. Wiley-Blackwell; 2001. ISBN: 10: 0471489972.
[12] Bahaj AS, Molland AF, Chaplin JR, Batten WMJ. Power and thrust measurements of marine current turbines under various hydrodynamic flow conditions in a cavitation tunnel and a towing tank. Renewable Energy 2007;32:407–26.
[13] Myers LE. Operational parameters of horizontal axis marine current turbines. Thesis. School of Civil Engineering and the Environment, University of Southampton; 2005.
[14] Builtjes PJ. The interaction of windmill wakes. In: Proceedings of the 2nd Int. Symposium on wind energy systems, Amsterdam 1978.
[15] Myers LE, Bahaj AS. Experimental analysis of the flowfield around horizontal axis tidal turbines by use of scale mesh disk rotor simulators. Ocean Engineering 2010;37:218–27.

[16] Myers LE, Bahaj AS. An experimental investigation simulating flow effects in first generation marine current energy converter arrays. Renewable Energy 2012;37:28–36. http://dx.doi.org/10.1016/j.renene.2011.03.043.
[17] Milne I, Sharma RN, Flay RGJ, Bickerton S. Characteristics of the turbulence in the flow at a tidal stream power site. Philosophical Transactions of the Royal Society A: Mathematical, Physical and Engineering Sciences 2013;371(1985).
[18] Lohrmann A, Cabrera R, Kraus NC. Acoustic Doppler velocimeter (ADV) for laboratory use. In: Proceedings of the symposium on fundamentals and advancements in hydraulic measurements and experimentation, ASCE 1994. p. 351–65.
[19] Voulgaris G, Trowbridge JH. Evaluation of the acoustic Doppler velocimeter (ADV) for turbulence measurements. Journal of Atmospheric and Oceanic Technology 1998;15:272–89.
[20] Cea L, Puertas J, Pena L. Velocity measurements on a highly turbulent free surface flow using ADV. Experimental Fluids 2006;42:333–48.
[21] Vermeer LJ, Sorensen JN, Crespo A. Wind turbine wake aerodynamics. Progress in Aerospace Sciences 2003;39:467–510.
[22] Thomson J, Polagye B, Richmond M, Durgesh V. Quantifying turbulence for tidal power applications. In: MTS/IEEE Seattle, OCEANS 2010, September 20 2010. ISBN:13: 9781424443321.